Bistability and relaxor ferrimagnetism in off-stoichiometric NiCrO3

Bistability and relaxor ferrimagnetism in off-stoichiometric $NiCrO_3$

A F Kusmartseva,[1,3] A M Arevalo-Lopez, [2] M Halder[3] and J P Attfield[2]

[1] Department of Physics, Loughborough University, Loughborough, LE11 3TU, United Kingdom

[2]Centre for Science at Extreme Conditions and School of Chemistry, University of Edinburgh, Mayfield Road, Edinburgh EH9 3JZ, United Kingdom

[3] Physik Department, Technische Universität München, Garching 85748, Germany

Abstract:

$NiCrO_3$ has been proposed as a likely candidate for antiferromagnetic half metallic behaviour. A sample prepared at high pressure adopts the corundum structure with Ni/Cr cation disorder, and is found to have off-stoichiometric composition $Ni_{0.80}Cr_{1.20}O_3$. This material shows complex local magnetic ordering phenomena at temperatures below 120 K but without any long range spin order observed by neutron diffraction. The transition to local ferrimagnetism occurs at 50 – 100 K, with two distinct regimes at T_{C1} = 95 and T_{C2} = 53 K evidencing electronic phase separation driven by variations in local composition or cation order. At low temperature the system undergoes a further transition at T_{C3} = 22 K, assigned to orbital order of low spin Ni^{3+} cations, that results in a substantial increase in magnetic anisotropy. $Ni_{0.80}Cr_{1.20}O_3$ is a bistable relaxor ferrimagnet where magnetic properties are linked to the local lattice strain manifold that switches between two distinct charge distributions or Ni^{3+} spin states.

1. Introduction:

Magnetic materials with significant conductivity are of interest for their electronic band structure and applications in spintronic technologies. Magnetic half-metals are of particular importance for sensors and functional spintronic devices.[1,2,3] These materials have spin-polarised electronic densities of states at the partially gapped Fermi level. Antiferromagnetic (AFM) half metals are additionally characterised by a fully compensated spin which allows spin-polarized current generation without exhibiting external macroscopic magnetic field.[4,5] The lack of stray fields renders these types of materials as perfect candidates for magnetic sensors, probes and memory storage units. Significant effort has been dedicated to the search for antiferromagnetic half metals, particularly those exhibiting the AFM transition near 300K.[6,7] To date, no suitable compound system has been successfully synthesised, although numerous material families have been explored theoretically.

$NiCrO_3$ has been proposed as a likely candidate for an antiferromagnetic half metal (a compensated half-metallic ferrimagnet).[8,9] Ordering of Ni^{2+} and Cr^{4+} cations with opposed S = 1 spins could give rise to ferrimagnetism with a very small net magnetisation, and Cr^{4+}-based perovskites such as $CaCrO_3$ and $SrCrO_3$ are metallic or near-metallic conductors.[10,11,12,13,14] Ni/Cr electronic transfer is another possibility in $NiCrO_3$, and the alternative Ni^{3+}/Cr^{3+} configuration could also lead to compensated ferrimagnetism for high spin (HS) Ni^{3+}, where both cations have S = 3/2 states, but octahedral Ni^{3+} may also have the low spin (LS) S = 1/2 state in oxide lattices and is potentially subject to Jahn-Teller distortion. Hence $NiCrO_3$ offers charge, orbital, spin and spin-state degree of freedoms and so is of fundamental interest for transition metal oxides physics. Electronic structure calculations[8,9] predict that the material has a substantial energy gap in the spin up channel (~3 eV) and a near vanishing energy gap in the spin down channel, satisfying the conditions necessary for a half metal, or a magnetic narrow-band semiconductor. An early experimental report suggested that $NiCrO_3$ has an antiferromagnetic phase transition near 250 K,[15] but follow-on studies are not reported. Here, we report the high pressure synthesis and structural, electrical, magnetic and thermal properties of $NiCrO_3$ which provide a detailed picture of the physical and structural behaviours of this material.

2. Experimental

Polycrystalline samples of $NiCrO_3$ were synthesized at 11 GPa pressure and 1100 °C inside a multi-anvil Walker press apparatus. Disk pellets of approximate dimensions 2 x 0.5 mm were cut from the sintered products for physical measurements, and other product was ground to a

powder. Powder x-ray diffraction showed that a rhombohedral corundum-related phase was present plus a trace of NiO.

Powder neutron diffraction data from a 60 mg sample of $NiCrO_3$ were collected at 2, 50, 100 and 150 K with a neutron wavelength of 2.418 Å using instrument D20 at the ILL facility. The magnetisation measurements were carried out using a Vibrating Sample Magnetometer (VSM) system and a Quantum Design Magnetic Properties Measurement System (QD MPMS) collectively. The electrical and specific heat properties were studied by a Quantum Design Physical Properties Measurement System (QD PPMS).

3. Results

3.1 Powder neutron diffraction

Neutron diffraction provides high nuclear scattering contrast between Cr and Ni enabling cation order and composition to be assessed critically. Fits of the cation-disordered corundum type (space group $R\bar{3}c$) and cation-ordered $LiNiO_3$ (R3c) and ilmentite ($R\bar{3}$) structures to the data were compared. Neither of the cation-ordered arrangements significantly improved the fit relative to the corundum type, so the latter model was taken as the best description of the average structure and refinement results are shown in Table I and Fig. 1(a). The sample was found to be off-stoichiometric with a refined composition of $Ni_{0.80(2)}Cr_{1.20}O_3$. 14 wt % of a secondary NiO phase was also observed, consistent with the Ni-deficiency of the main product. NiO is antiferromagnetic with a Neel temperature of 520 K and thus does not contribute to the magnetic phenomena observed below 300 K reported later.

The above structural study reveals that there are two main types of chemical disorder in the present $NiCrO_3$ sample – the inherent cation site disorder characteristic for a corundum structure where all cation sites are symmetry-equivalent[16] and the off-stoichiometry disorder due to excess of Cr. The latter non-stoichiometry in the present sample of $NiCrO_3$ likely suppresses any long range cation-ordering in this material.

No changes in the Bragg scattering such as from a lattice distortion were observed between 2 and 150 K, and no magnetic diffraction peaks were seen so no long-range spin order is evident. However, changes in diffuse background scattering are observed in the intensity differences between profiles at T = 2, 50, or 100 K, and the 150 K profile, as shown in Fig. 1(b). Plots of the intensity differences relative to the 150 K pattern $I(T\text{- }150\text{ K})$ show a growth

of short range spin-spin correlations between 100 and 50 K, with little further change between 50 and 2 K.

3.2 Magnetisation

$NiCrO_3$ exhibits unusual magnetism, the most obvious signature of which is the development of a broad ferromagnetic response below 120 K (Fig. 2). Confirmation of the ferromagnetism is observed in the divergence between the zero-field cooled (zfc) and field cooled (fc) magnetisation that sets in at the same temperature. At high fields the divergence is shifted to lower temperatures. The difference between zfc and fc data is due to ferromagnetic domain formation. The broad character of the transition reflects the intrinsic and off-stoichiometry induced disorder. Our results do not support the antiferromagnetic transition reported near 250 K in an early study.[15]

Magnetisation-field studies confirm the ferro- or ferri- magnetic character of this phase (Fig. 3). A weak ferromagnetic hysteresis emerges between near 100 K and the magnetisation saturates below ~50 K. Magnetic hysteresis broadens significantly below 20 K suggesting increased magnetic anisotropy or the hardening of the magnetic axis in the bulk phase at low temperatures. The small saturated moment of ~0.07 μ_B/formula unit (f.u.) at 2 K suggests that some local cation ordering or segregation occurs within the $NiCrO_3$ sample. Similar small net magnetisations are observed in other ostensibly disordered magnetic oxides such as $SrCr_{1-x}Ru_xO_3$ solid solutions.[17]

The AC magnetisation of $NiCrO_3$ results reveal additional surprising properties, as both real and imaginary parts of the AC magnetisation show three sharp peak features at low temperatures – at T_{C1} = 95, T_{C2} = 53 and T_{C3} = 22 K (Fig. 4). The AC magnetisation results demonstrate that varying magnetic energy scales are present in the system. The highest-temperature onset of ferromagnetism occurs at the position of the first peak at T_{C1} = 95 K, while the lower limit for the transition is signalled by the second peak at T_{C2} = 53 K. Structural disorder and local variations in stoichiometry are likely to be responsible for the broad range of magnetic interactions. The lowest temperature peak at T_{C3} = 22 K coincides with the increase in coercivity observed in the hysteresis study. A likely explanation is that this is due to local orbital ordering resulting from Jahn-Teller distortions of LS Ni^{3+} sites causing hardening of the magnetic axis.

To investigate possible spin glass dynamics in this system excitation frequency was varied between 10 Hz and 10 kHz. The frequency dependence of the AC magnetisation in $NiCrO_3$ is

summarized in Fig.8. The real part of AC magnetisation M' shows three peaks where only the peak at 95K demonstrates marginal frequency dependence, and is enhanced at an approximate rate of 1K/10kHz (Fig. 8a). The other two peaks at 22K and 53K remain invariant with frequency. Notably, the peaks are rather broad, which may give rise to some uncertainty in the frequency analysis. The absence of significant frequency-induced changes in M' eliminates bulk spin-glass behaviour. The imaginary part of the AC magnetisation – M'' shows moderate frequency dependence on all peaks (Fig. 8b). The peak at 95K follows positive frequency dependence both in the real M' and the imaginary M'' parts of the AC magnetisation. This may be indicative of rapid magnetic dynamics associated with this energy scale.

3.3 Electrical resistivity

The electrical resistivity of a sintered bar of $NiCrO_3$ was obtained using a DC resistivity method for the temperature range 2 – 300 K (Fig. 5). No magnetic field dependence was observed in fields up to 9 T. The temperature dependence of the resistivity is positive, and resistivity varies as $\exp(-\Delta/k_B T)$ over a wide temperature range 80 – 300 K. The band gap of Δ= 11 meV shows that $NiCrO_3$ is a narrow band gap semiconductor, or may be metallic with grain boundary resistances in the polycrystalline sample giving rise to the positive temperature-dependence.

At temperatures 80 K the resistivity deviates from the activated-semiconductor dependence, suggesting that other mechanisms are active in the magnetic regime. Low-dimensional (1D and 2D) variable range hopping (VRH) did not provide a suitable fit to the data at lower temperatures, indicating that more complex scattering processes are responsible for the super-logarithmic temperature dependence in the electron transport. Theoretical calculations indicate the Coulomb enhanced spin-orbit coupling may play a role here.[18]

3.4 Heat capacity

The heat capacity measurements were performed on sintered grains of $NiCrO_3$ with a total mass of 1.5 mg. The total heat capacity shows monotonic temperature dependence over the entire temperature range 2 – 300 K (Fig. 6), with no peak-like features to indicate first-order phase transitions. An estimated lattice contribution was subtracted from the total signal, using a standard Debye model with fitting parameter θ_D = 825 K. The resulting magnetic heat capacity shows unusual behaviour with a broad peak developing near T_{C1} = 95 K (see Fig.

6(a)). The maximum slope shown by the derivative of the magnetic heat capacity is close to T_{C2} = 53 K (see Fig. 6(b)). An additional shoulder develops below T_{C3} = 22 K (see Fig. 6(c)). Hence the features in the magnetic heat capacity corroborate the three peaks observed in the AC magnetisation of $NiCrO_3$ as shown on Figure 7.

The heat capacity was studied as a function of magnetic field in the range 0 – 9T to further clarify the role of lattice and phonons in $NiCrO_3$ (Fig. 9a). Unexpectedly, the full heat capacity demonstrates little to no field dependence, with only minor changes between 0T and 9T at high temperatures (Fig.9a). In particular, for temperatures exceeding ~120K there is a slight reduction (~2%) in the heat capacity at 9T. This may be attributed to the suppression of soft phonon modes. It is unclear whether the effect may have relevance to the magnetic transitions that occur below this temperature scale.

In order to probe the true semiconducting or metallic character in $NiCrO_3$ the temperature dependence of the total heat capacity signal was investigated in depth. The results were analysed within a standard Sommerfeld model for metals $C = \gamma T + AT^3$. To test the premise, the behaviour of C/T is reported as a function of quadratic temperature T^2 in the range 2 – 300K (Fig. 9b). In accordance with the Sommerfeld predictions the C/T shows near linear behaviour as a function of T^2 at low temperatures <10K. Furthermore, the C/T signal extrapolates to a non-zero value at zero temperature (T=0K), giving a Sommerfeld coefficient of γ=13mJ/(mol-K^2). The moderately high value of the Sommerfeld coefficient may suggest the presence of electronic correlations in the system. These combined results support the scenario that $NiCrO_3$ is likely to be locally metallic at least at low temperatures.

4. Discussion and conclusion

The present study shows that synthesis of $NiCrO_3$ is not straightforward as high pressures are required and the material tends to be Cr-rich with NiO formed as a secondary phase. Neutron diffraction analysis of the structure demonstrates that the present material is off-stoichiometric with composition $Ni_{0.80}Cr_{1.20}O_3$ and crystallizes in a cation-disordered corundum structure. This is equivalent to Ni-doping of corundum-type Cr_2O_3. Investigation of more stoichiometric materials will be required to discover whether Ni/Cr cation order is possible and what the charge and spin states are.

Despite the presence of intrinsic and off-stoichiometry cation disorder, the present $Ni_{0.80}Cr_{1.20}O_3$ sample shows complex ferrimagnetic behaviour with a small magnetisation of

~0.07 μ_B/f.u. that evidences local cation and spin orders, although no long range spin order is observed by neutron diffraction down to 2 K.

The onset of ferrimagnetism in $Ni_{0.80}Cr_{1.20}O_3$ occurs across a broad range of temperatures between 120 and 40 K which evidences a wide range of local interactions. However, the presence of two broad but well defined peaks in the AC magnetisation at T_{C1} = 95 K and T_{C2} = 53 K shows that two distinct types of region are present. This bistability is most likely to reflect electronic or magnetic phase segregation. One possibility is that different charge states are present, so some regions have Ni^{2+}/Cr^{4+} while others have the Ni^{3+}/Cr^{3+} configuration. An alternative explanation is that the Ni^{3+} spin configuration changes between HS and LS in different regions. The segregation could be driven by small differences in the Cr/Ni content based on the ionic sizes. The ionic radii are 0.615 Å for Cr^{3+}, 0.60 Å for HS Ni^{3+}, and 0.56 Å for LS Ni^{3+}, so while Ni-rich regions might favour LS Ni^{3+}, the lattice expansion in Cr-rich regions may switch to HS Ni^{3+}. The additional magnetic transition at T_{C3} = 22 K that coincides with the increase in coercivity evidences local orbital ordering and hence strongly suggests that at least one of the two magnetic components contains LS Ni^{3+}, as this is the only available cation with an E-type (doubly degenerate) electronic ground state that is prone to strong Jahn-Teller distortion. Both theoretical[19] and experimental[20] approaches indicate that local Cr-rich regions have a significant effect on ferromagnetic interactions.

The ferrimagnetism in this system is likely to be linked to electronic bistability as discussed above but Coulomb enhanced crystal field splitting may also play a role, as suggested by the anomalous electrical resistivity behaviour at low temperatures. Recent theoretical predictions showed that Coulomb interactions are important in the related material $PdCrO_3$ that displays half-metal ferrimagnetic properties.[21] A similar result has also been calculated for isostructural $NiMoO_3$, where the ferromagnetic half-metallicity has been attributed to Coulomb enhanced spin orbit coupling.[22]

Earlier works have reported relaxor ferromagnetic behaviour in Cr-doped $Nd_{0.5}Ca_{0.5}MnO_3$ perovskite which had been explained by a model of ferromagnetic clusters embedded in a charge-ordered antiferromagnetic matrix.[23] The present $Ni_{0.80}Cr_{1.20}O_3$ system may be considered as a corundum-structured electronic analogue of such a ferromagnetic relaxor perovskite. However, it is important to note that the $NiCrO_3$ pervoskite remains a hypothetical structural phase, and the search for it continues.

In summary $Ni_{0.80}Cr_{1.20}O_3$ may be described as a bistable relaxor ferrimagnet,[24] where magnetic properties are linked to the local lattice strain manifold that switches between two distinct charge distributions or Ni^{3+} spin states. Local probes of magnetism such as μSR spectroscopy will be needed to explore this material further, and preparation of stoichiometric $NiCrO_3$ to explore potential cation order and bulk ferrimagnetism and half-metallicity remains a challenge.

Acknowledgments

We gratefully acknowledge the ILL staff at the D20 facility for assistance with collection of the neutron diffraction data. We would also like to thank Andreas Bauer for his help with the magnetic susceptibility and heat capacity measurements. The work was supported by the Alexander von Humboldt Foundation and the Engineering and Physical Science Research Council (EPSRC).

References

[1] Son Y W, Cohen M L and Louie S G 2006 *Nature* **444**, 347

[2] Nakatsuji S, Kiyohara N and Higo T 2015 *Nature* **527**, 212

[3] Resta R 2010 *Journal of Physics: Condensed Matter* **22**, 12, 123201

[4] Hu L, Wu X and Yang J 2016 *Nanoscale* **8**, 12939-12945

[5] Si C, Zhou J, and Sun Z 2015 *ACS applied materials & interfaces* **7**(31), 17510-17515

[6] Shahjahan M and Oguchi T 2016 *Journal of Physics and Chemistry of Solids* **93**, 157-162

[7] Meneghini C, Di Matteo S, Monesi C, Neisius T, Paolasini L, Mobilio S, Natoli C R, Metcalf P A and Honig J M 2009 *Journal of Physics: Condensed Matter* **21**, 35, 355401

[8] Qian Y, Wu H, Liu Y, Lu J, Lu R, Tan W, Deng K, Xiao Ch and Lu G 2013 *Solid State Communications* **170**, 24-29

[9] Lee K-W and Pickett W E 2011 *Phys. Rev. B* **83**, 180406(18)

[10] Zhou J S, Jin C Q, Long Y W, Yang L X and Goodenough J B 2006 *Phys. Rev. Lett.* **96**, 046408

[11] Ortega-San-Martin L, Williams A J, Rodgers J, Attfield J P, Heymann G and Huppertz H 2007 *Phys. Rev. Lett.* **99**, 255701

[12] Komarek A C, Streltsov S V, Isobe M, Moller T, Hoelzel M, Senyshyn A, Trots D, Fernandez-Diaz M T, Hansen T, Gotou H, Yagi T, Ueda Y, Anisimov V I, Gruninger M, Khomskii D I and Braden M 2008 *Phys. Rev. Lett.* **101**, 167204

[13] Castillo-Martinez E, Duran A and Alario-Franco M A 2008 *J. Solid State Chem.* **181**, 895-904

[14] Alario-Franco M A, Castillo-Martinez E and Arevalo-Lopez A M 2009 *High Pressure Research* **29**, 254

[15] Chamberland B L and Cloud W H 1969 *Journal of Applied Physics* **40**, 434

[16] Hoel C A, Gallardo-Amores J M, Moran E, Alario-Franco M A, Gaillard J F and Poeppelmeier K R 2010 *J. Am. Chem. Soc.* **132**, 16479-16487

[17] Rodgers J A, Williams A J, Martinez-Lope M J, Alonso J A and Attfield J P 2008 *Chem. Mater.* **20**, 4797-4799

[18] Wu H 2013 *New Journal of Physics* **15**, 023038

[19] Da Silva J L F, Dalpian G M and Wei S H 2008 *New Journal of Physics* **10**, 113007

[20] Kobayashi M *et al* 2008 *New Journal of Physics* **10**, 055011

[21] Jin H S and Lee K W 2011 *Phys. Rev. B* **84**, 172405

[22] Wang J and Wu Z J 2012 *Appl. Phys. Lett*. **101**, 042414

[23] Kimura T, Tomioka Y, Kumai R, Okimoto Y and Tokura Y 1999 *Phys. Rev. Lett.* **83**(19), 3940

[24] Battle P D, Evers S I, Hunter E C and Westwood M 2013 *Inorg. Chem.* **52**, 6648-6653

Table 1. Refined cell parameters and atomic parameters for the corundum-type model (space group $R\bar{3}c$) of $NiCrO_3$ using 150 K powder neutron diffraction data. The cell parameters are a = 4.9195(1) Å and c = 13.4619(5) Å (R_b = 3.09%, R_f = 3.86%, R_p = 2.85%, R_{wp} = 3.82%).

Atom	x	y	z	B_{iso} (Å^2)	Occupancy
Cr/Ni	0	0	0.3491(2)	1.06(4)	0.60(1)/0.40
O	0.6905(4)	0	0.25	1.06	1.0

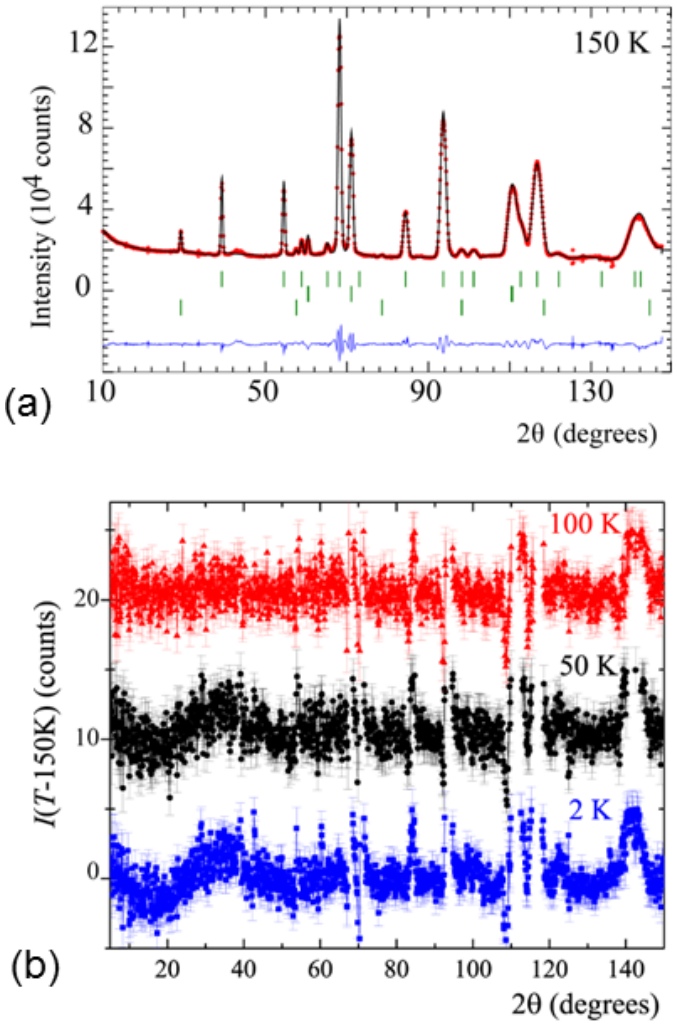

Figure 1 Powder neutron diffraction data for $NiCrO_3$. (a) Fit to the 150 K data. Reflection markers from top to bottom correspond to the corundum-type $NiCrO_3$ phase, NiO, and the magnetic structure of NiO. (b) The differences between neutron diffraction profiles collected at 2, 50 and 100 K, and the 150 K data. The 50 and 100 K difference profiles are offset by 10 and 20 counts respectively.

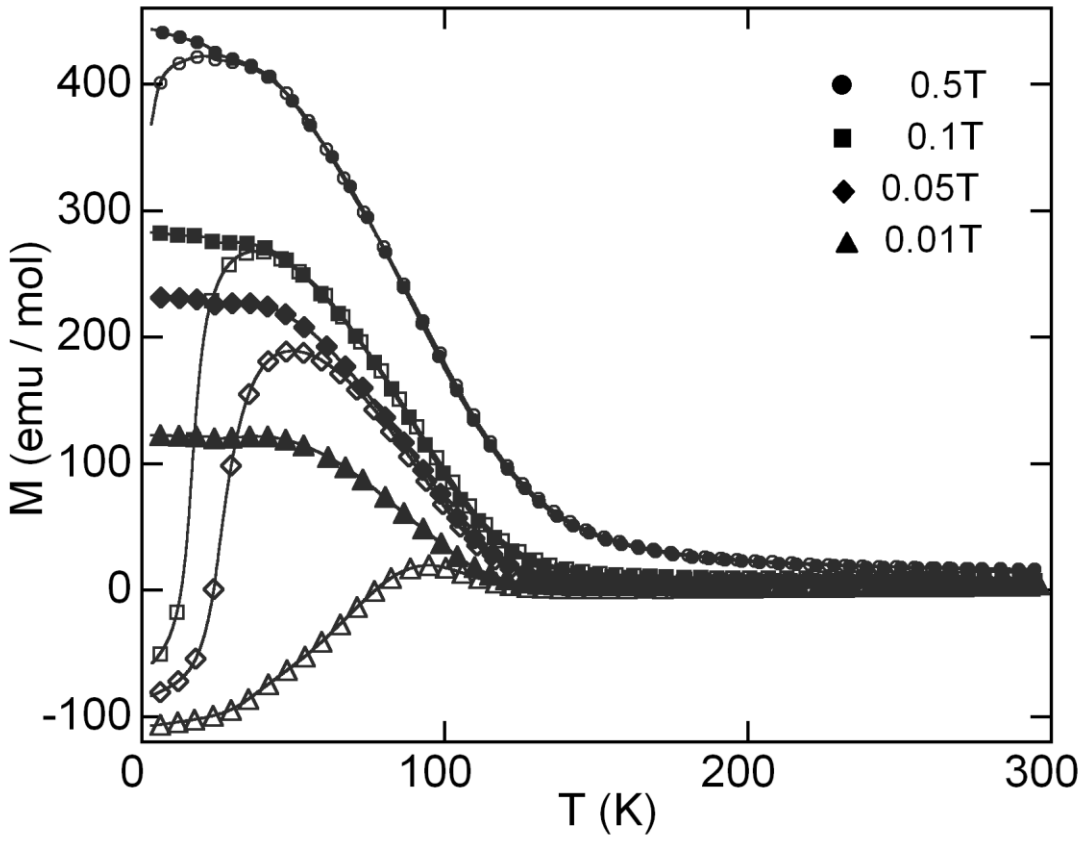

Figure 2 The magnetisation *M* of $NiCrO_3$ as a function of temperature under field-cooled (filled symbols) and zero-field cooled (open symbols) conditions. The measurement fields are 0.5 T (circles), 0.1 T (squares), 0.05 T (triangles) and 0.01 T (diamonds). A broad deviation between the zfc and fc magnetisation sets in below a temperature of 120 K and progresses to lower temperatures with increased magnetic field.

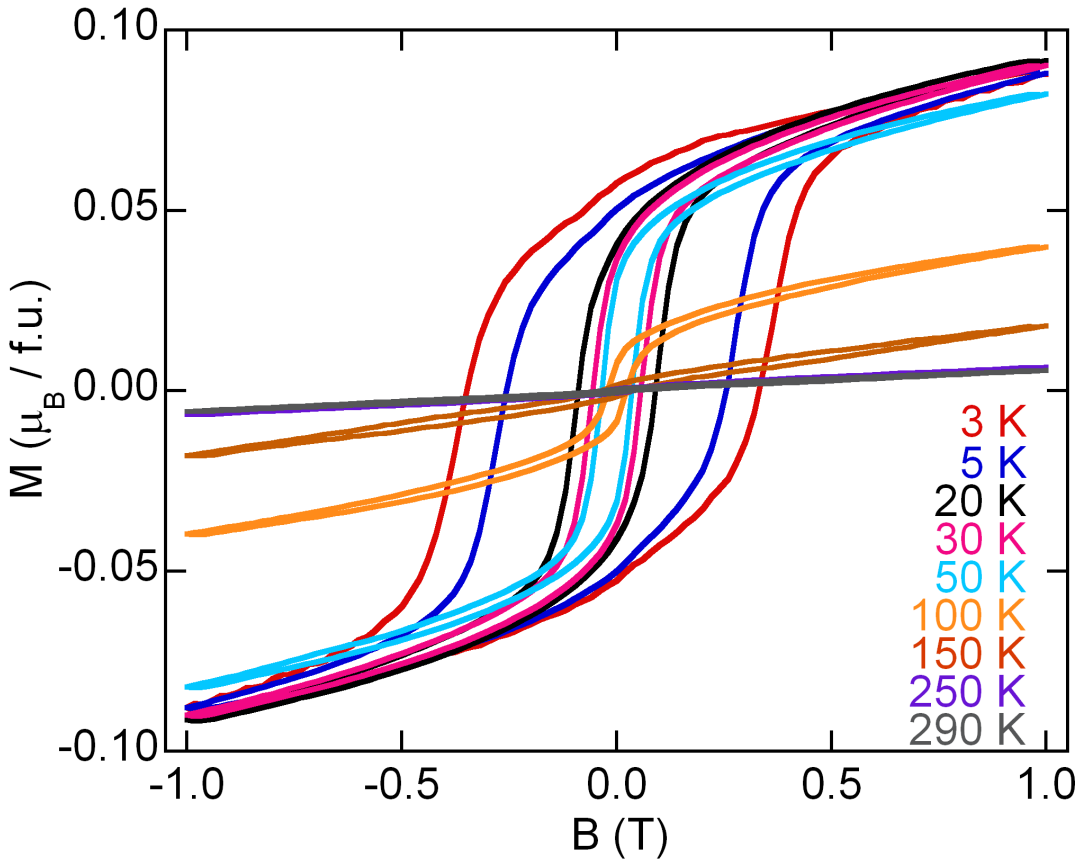

Figure 3 The magnetisation *M* as a function of field *B* at temperatures in the range 3 – 300 K. Magnetic hysteresis appears for temperatures of 150 K and below. Magnetisation increases substantially below 50 K and coercivity increases below 20 K, indicating magnetic hardening that may accompany local orbital ordering of LS Ni^{3+}.

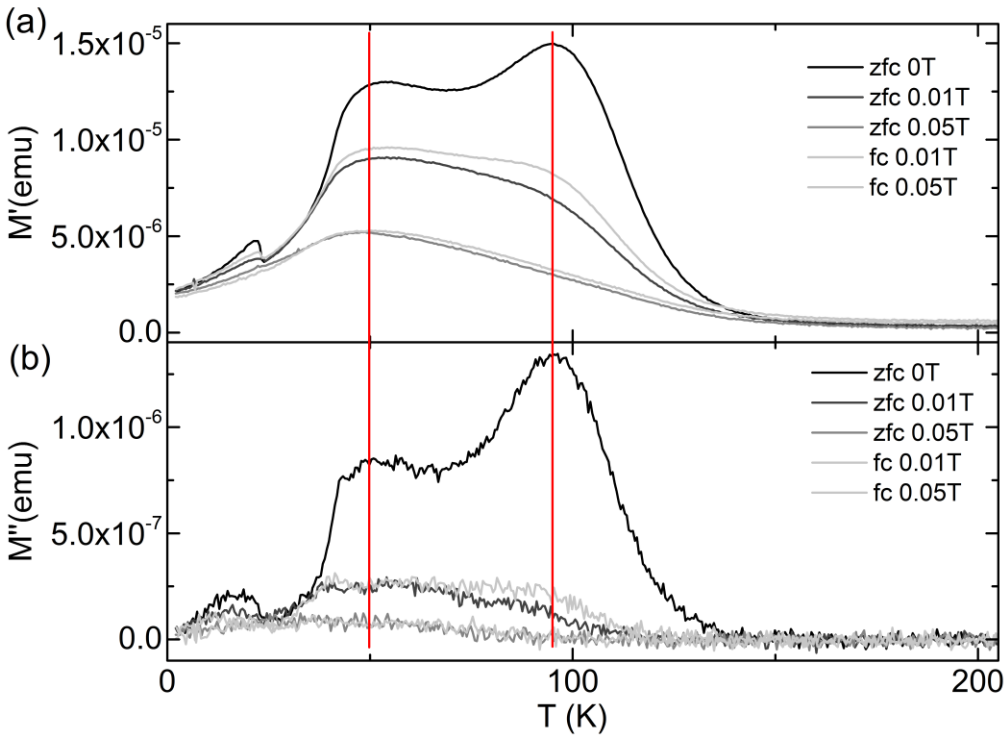

Figure 4 AC magnetisation measurements for $NiCrO_3$. (a) The real parts of AC magnetisation – *M*' as a function of temperature. The black-dark-grey lines denote the zero-field cooled (zfc) data, and the light grey lines indicate the field-cooled (fc) results. The measurement frequency is $f = 997$ Hz and fields up to 0.0 5T were applied. (b) The imaginary parts of AC magnetisation – *M*'' as a function of temperature. The darker lines denote the zfc data, and the lighter lines indicate the fc results. Both parts of the AC magnetisation show three pronounced peaks – at $T_{C1} = 95\pm2$ K, $T_{C2} = 53\pm2$ K and $T_{C3} = 22\pm2$ K in the zfc results. The AC magnetisation data indicates strong magnetic dynamics of the peak at $T_{C2} = 53$ K – namely near invariance with applied field and soft dynamics – or easily suppressed with applied fields at $T_{C1} = 95$ K and $T_{C3} = 22$ K. The results for *M*' were insensitive to frequency variation up to 10 kHz, exempting spin-glass dynamics. These results are consistent with the changes in the neutron diffraction profiles observed at 50 K.

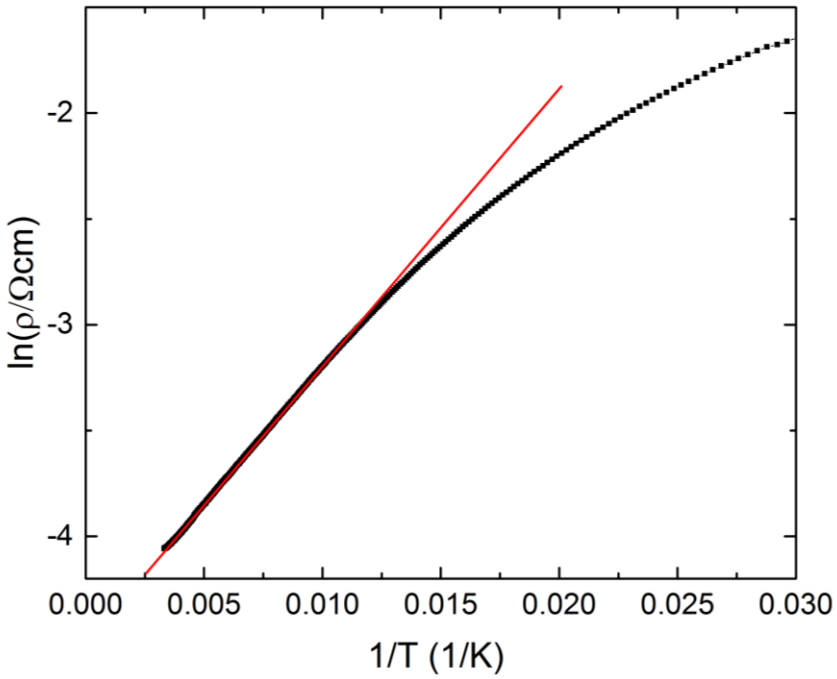

Figure 5 Resistivity in zero magnetic field (under zfc conditions) as a function of temperature. The resistivity follows a logarithmic temperature dependence ln(ρ)~1/T for temperatures between 80 and 300 K, with a band gap energy of 11 meV. The resistivity increases non-logarithmically for temperatures below 80 K but a standard variable range hopping (VRH) model does not apply.

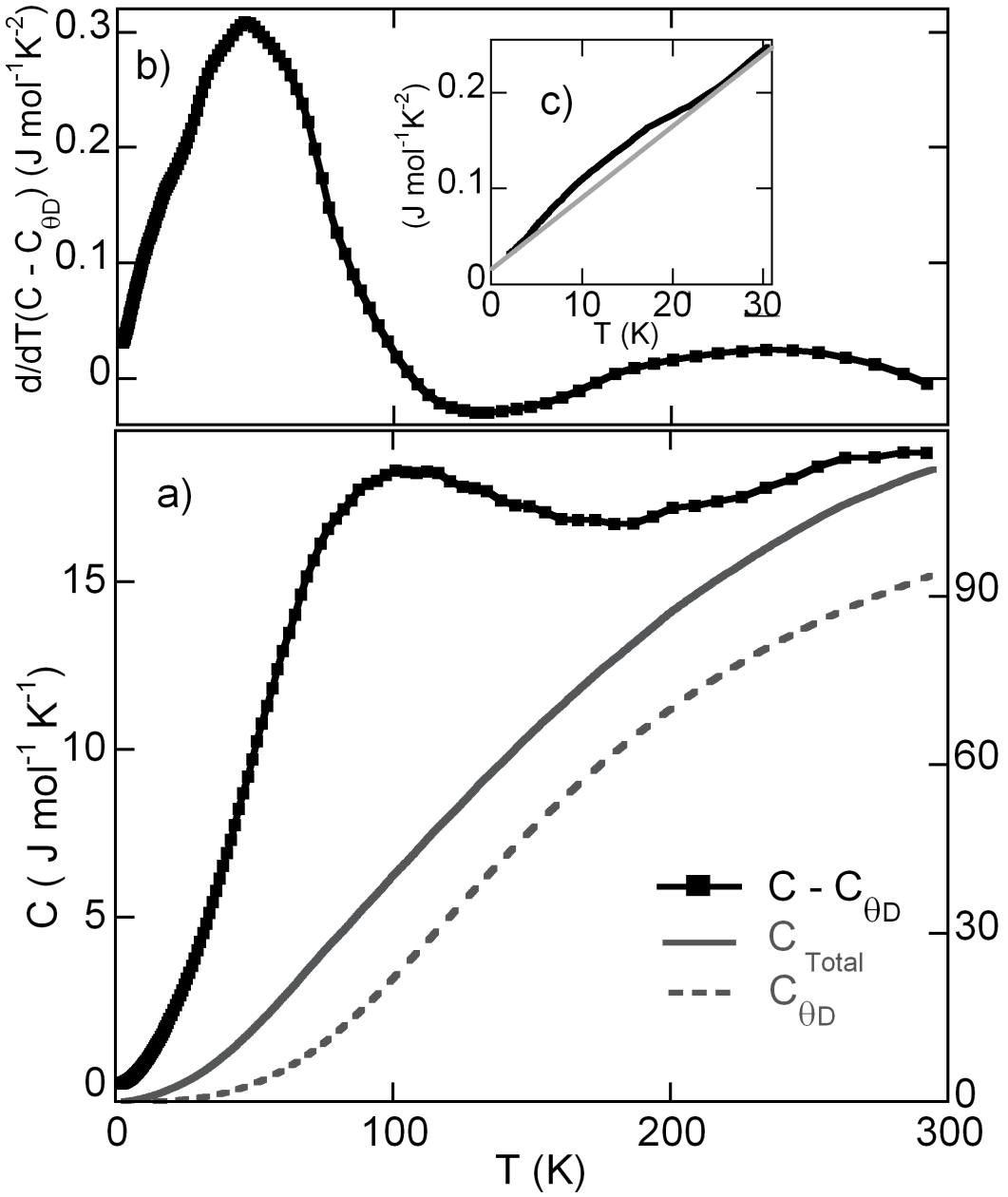

Figure 6 Heat capacity results for $NiCrO_3$. (a) The total measured heat capacity C and Debye heat capacity $C_{\theta D}$ calculated for $\theta_D = 825$ K (right scale); and the electronic heat capacity $C_{el} = C - C_{\theta D}$ (left scale) with a prominent peak at 85 ± 5 K. (b) The derivative of the electronic heat capacity C_{el} exposes a sharp peak at 47 ± 5 K. The inset (c) shows a small increase in the weight of the thermal derivative of the electronic heat capacity below 20 K.

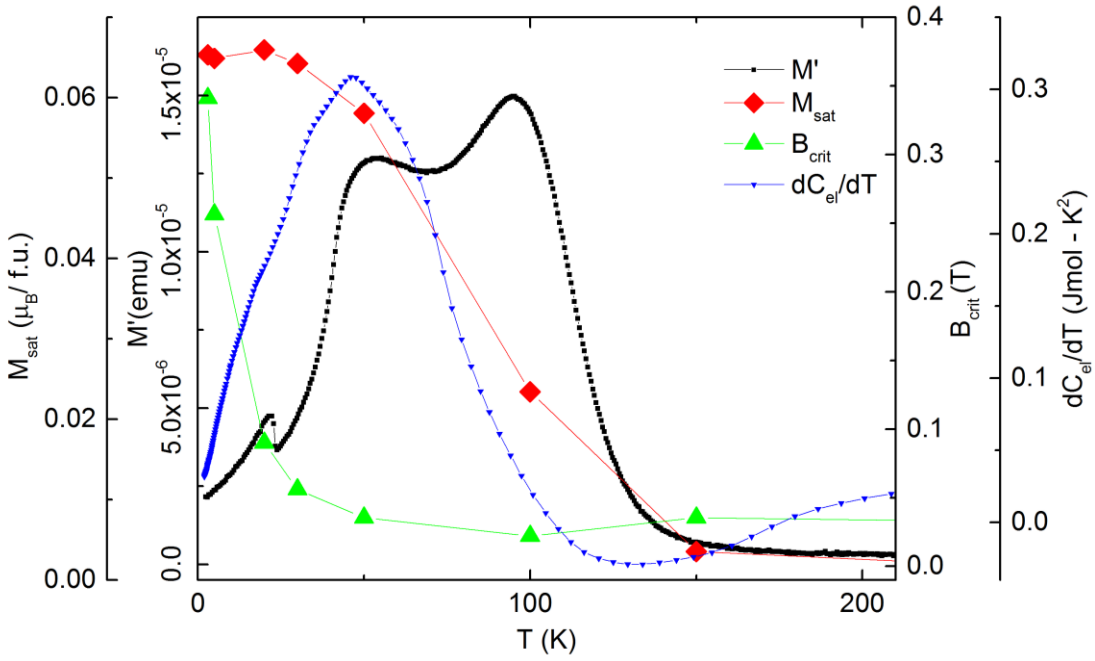

Figure 7 Combined master plot of physical measurements for $NiCrO_3$ showing the real part of AC magnetisation M'; temperature derivative of the electronic heat capacity dC_{el}/dT; saturation magnetisation M_{sat}; and the coercive field B_{crit}. These properties illustrate the complex local magnetic ordering phenomena at temperatures below 120 K. The transition to local ferrimagnetism occurs at $T_C \sim 50 - 100$ K, with two distinct regimes at 53 and 95 K evidencing some electronic phase separation driven by variations in local composition or cation order. At low temperature the system undergoes a further transition at $T_{C3} = 22$ K, potentially due to orbital order of LS Ni^{3+} cations, that results in substantial magnetic hardening as seen in the sharp rise of the coercive field B_{crit}.

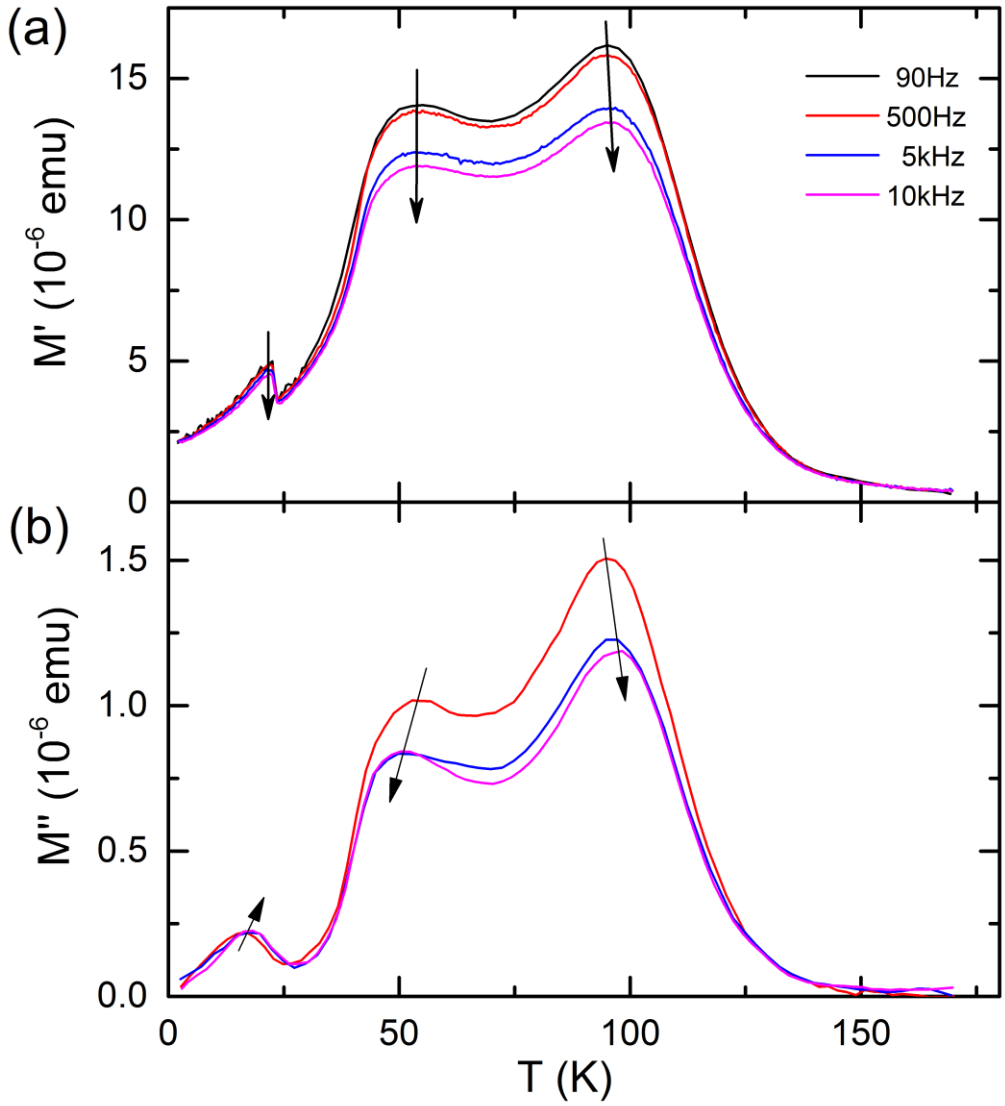

Figure 8 Frequency dependence of the AC magnetisation in the range of 90 Hz – 10 kHz. (a)The real part of AC magnetisation M' shows three peaks where only the peak at 95K demonstrates marginal frequency dependence, and is enhanced at an approximate rate of 1K/10kHz. The other two peaks at 22K and 53K remain invariant with frequency. Notably, the peaks are rather broad, which may induce some uncertainty in the frequency dependence analysis. (b) The imaginary part of the AC magnetisation – M'' shows moderate frequency dependence on all peaks. The peak at 95K displays positive frequency dependence both in the real M' and the imaginary M'' parts of the AC magnetisation. This may be indicative of rapid magnetic dynamics associated with this energy scale.

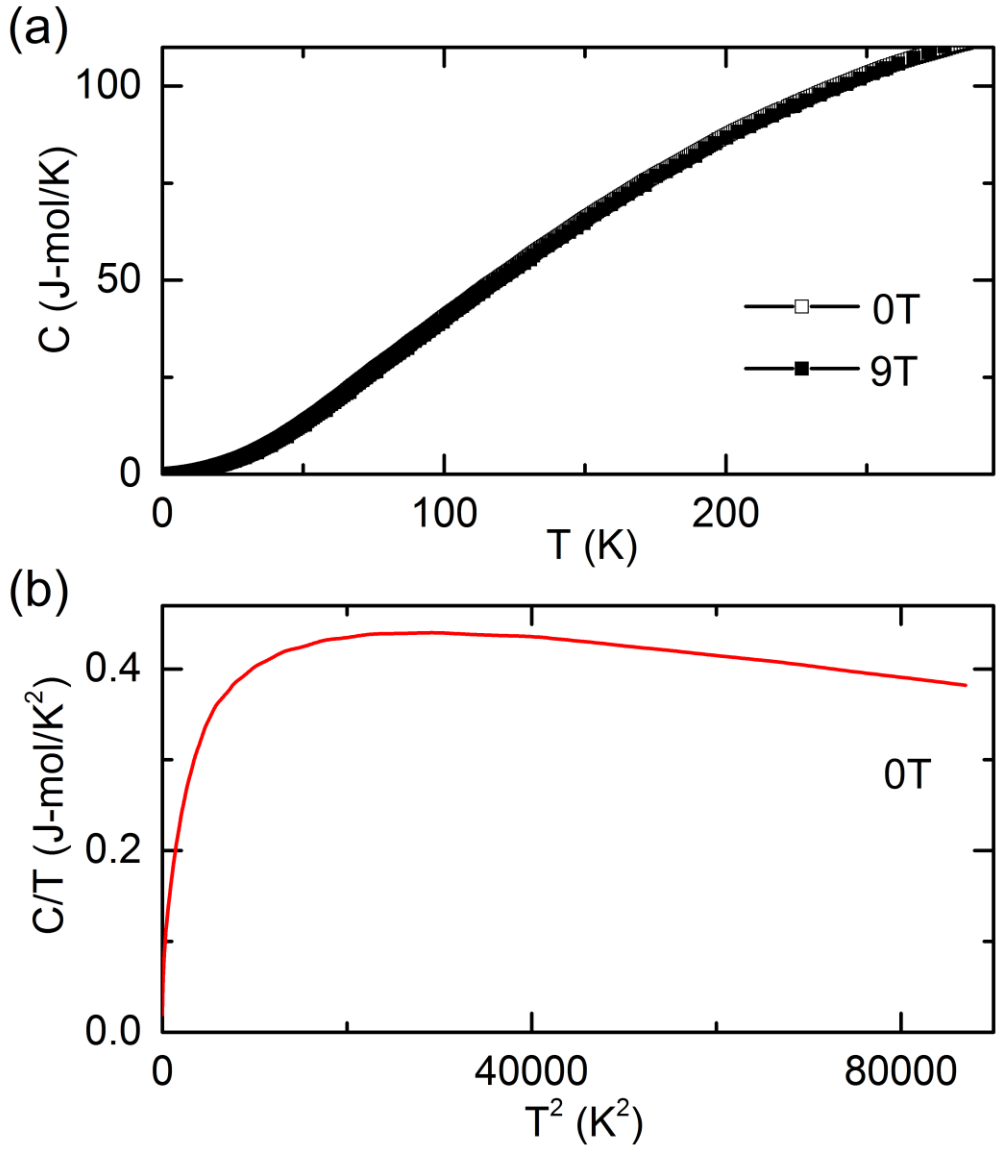

Figure 9 Temperature and field dependences of the total heat capacity signal. (a) The field dependence in C demonstrates minor changes between the 0T and the 9T. For temperature exceeding ~120K there is a slight reduction in the heat capacity at 9T. This may be attributed to the suppression of soft phonon modes. (b) The temperature dependence of C/T versus T^2 in the temperature range 2 – 300K. In accordance with the standard Sommerfeld model $C = \gamma T + AT^3$, the C/T signal is near-linear for <10K and extrapolates to a non-zero value at zero temperature, giving a Sommerfeld coefficient of γ=13mJ/(mol-K^2). The moderately high value of the Sommerfeld coefficient may suggest the presence of electronic correlations in the system. These combined results support the scenario that $NiCrO_3$ may be locally a metal at least at low temperatures.